Frontiers in Bioscience Landmark

Front. Biosci. (Landmark Ed) **2026**; 31(9): 55117
https://doi.org/10.31083/FBL55117

Original Research

Cysteine Residues Are Required for the Sliding Clamp-Dependent Endonuclease Activity of *Neisseria gonorrhoeae* MutL

Viktoriia Yu. Savitskaya[1,*], Mayya V. Monakhova[2], Daniil R. Bazanov[1], Anastasiia V. Litvinova[3], Viktoriia G. Snyga[1], Tatiana S. Oretskaya[2], Elena A. Kubareva[2]

[1]Department of Chemistry, Lomonosov Moscow State University, 119991 Moscow, Russia
[2]Belozersky Institute of Physico-Chemical Biology, Lomonosov Moscow State University, 119991 Moscow, Russia
[3]Department of Bioengineering and Bioinformatics, Lomonosov Moscow State University, 119234 Moscow, Russia
*Correspondence: svk1896@mail.ru (Viktoriia Yu. Savitskaya)
Academic Editor: Sung-Kun Kim
Submitted: 21 June 2026 Revised: 27 July 2026 Accepted: 18 August 2026 Published: 18 September 2026

Abstract

Background: *Neisseria gonorrhoeae* is a human pathogen that causes gonorrhea and employs a methylation-independent mismatch repair (MMR) pathway to regulate genomic stability and pilin antigenic variation. A key effector of this pathway, MutL, possesses ATPase, DNA-binding, and endonuclease activities, yet the molecular determinants governing its catalytic activity remain poorly understood. In particular, the functional relevance of conserved cysteine (Cys) residues located in the vicinity of the active site is unclear. **Methods:** We characterized a Cys free-variant of *Neisseria gonorrhoeae* MutL, in which all Cys residues were replaced with evolutionarily conserved substitutes, in comparison with the wild-type enzyme. ATPase activity, DNA-binding capacity, and endonuclease activity on supercoiled plasmid and linear DNA duplex substrates were assessed, and molecular dynamics simulations were performed to examine the conformational behavior of the C-terminal domain (CTD). **Results:** Cys substitutions do not markedly affect ATPase activity, DNA-binding capacity, or endonuclease activity on supercoiled plasmid substrates. However, the same amino acid substitutions led to an almost complete loss of sliding clamp-dependent endonuclease activity on linear DNA duplexes. Molecular dynamics simulations revealed that the cysteine substitutions alter the conformational dynamics of the CTD, displacing the catalytically active monomer from its productive orientation relative to the sliding clamp and thereby impairing sliding clamp-dependent endonuclease activity. **Conclusions:** These results indicate that Cys residues are not directly involved in catalysis but provide the conformational rigidity of the C-terminal domain required for productive engagement with the sliding clamp.

Keywords: methyl-independent mismatch repair; MutL endonuclease; β-clamp; *Neisseria gonorrhoeae*

1. Introduction

Maintenance of genome stability is a fundamental requirement for normal cell function. The mechanisms that safeguard the integrity of genetic information are headed by the excision DNA repair systems. Mismatch repair (MMR) is an evolutionarily conserved post-replicative pathway that corrects errors arising during DNA replication. In most prokaryotes, including the human pathogen *Neisseria gonorrhoeae*, MMR operates via a methylation-independent mechanism in which the key effectors are MutS and MutL. MutS recognizes mismatched base pairs in DNA, while MutL functions as a nicking endonuclease that introduces a single-strand break into the daughter strand, thereby initiating the repair process. Strand discrimination that means the ability to direct endonucleolytic cleavage specifically to the newly synthesized daughter strand, is achieved through interaction of the MutL C-terminal domain with the β-subunit of DNA polymerase III, which remains associated with the newly replicated DNA at the replication fork [1].

Neisseria gonorrhoeae, a Gram-negative obligate human pathogen that causes gonorrhea, is exhibiting growing resistance to multiple classes of antibiotics, underscoring the urgent need to identify new therapeutic targets [2]. Of particular interest is the role of MMR proteins in the antigenic variation of the pathogen: strains of *N. gonorrhoeae* lacking *mutS* or *mutL* genes display markedly elevated frequencies of antigenic variation of the major virulence factor, the surface protein pilin (PilE) [3,4,5]. This process is regulated by a G-quadruplex (G4) structure located upstream of the *pilE* promoter, which is required for the initiation of homologous recombination underlying pilin antigenic variation [6]. We have previously shown that *N. gonorrhoeae* MutL (ngMutL) displays enhanced binding affinity for G4 structures compared to a canonical DNA duplex, yet does not hydrolyze DNA within the quadruplex core, bypassing this noncanonical structure instead [7]. These findings reveal previously undescribed properties of ngMutL and suggest that, beyond its canonical role in mismatch correction, the protein may perform alternative functions through interaction with G4 elements—potentially

Copyright: © 2026 The Author(s). Published by IMR Press.
This is an open access article under the CC BY 4.0 license.

Publisher's Note: IMR Press stays neutral with regard to jurisdictional claims in published maps and institutional affiliations.

contributing to the regulation of pilin antigenic variation by a mechanism distinct from endonucleolytic processing.

NgMutL functions as a homodimer in solution, consistent with other bacterial MutL homologs [8]. Each monomer consists of 658 amino acid residues organized into two functional domains: an N-terminal ATPase domain (NTD, residues 1–324) and a C-terminal endonuclease domain (CTD, residues 458–658), connected by an unstructured linker region [9]. MutL homologs are multifunctional proteins possessing ATPase, DNA-binding, and endonuclease activities [10]. The ATPase and DNA-binding activities are localized in the NTD. Although the crystal structure of full-length ngMutL has not been resolved, three-dimensional models of NTD-ngMutL predicted by AlphaFold are available. The endonuclease function resides in the CTD, whose crystal structure was determined by Namadurai et al. (PDB: 3NCV) [9]. The catalytic center contains conserved motifs, including the metal-binding motif ^{491}DMHAAAERVNYE^{502}, which coordinates divalent metal ions during DNA hydrolysis, and the motif ^{517}QHLLIP^{522}, which mediates interaction with the β-subunit of DNA polymerase III (β-clamp) to enhance processivity during MMR. The CTD also contains a dimerization subdomain and a regulatory (outer) subdomain exposed to solvent [8]. The functional importance of specific residues within these motifs is well established: for instance, the double substitution D491N/E497Q in the metal-binding motif of MutL from *N. gonorrhoeae* substantially reduces DNA hydrolysis efficiency. At the same time single substitution D467N MutL *Pseudomonas aeruginosa* (the analogue of D491N of MutL from *N. gonorrhoeae*) also reduces DNA hydrolysis efficiency [8,11].

ATPase activity, DNA-binding capacity, endonuclease activity on plasmid substrates, and β-clamp-stimulated nicking of linear DNA substrates have been previously demonstrated for ngMutL [7,12,13]. The molecular determinants governing the efficiency of this sliding clamp-dependent endonuclease activity had not been fully established. Recently, the crystal structure of the CTD-ngMutL: β-clamp complex revealed that the endonuclease domain "sits" transversely across the β-clamp ring, with strand discrimination achieved through precise geometric positioning of the daughter strand towards one of the two active sites [1]. However, the contributions of specific residues within the CTD to the conformational integrity required for productive complex formation with the sliding clamp remained unknown.

Notably, many MutL homologs lose activity *in vivo* upon substitution of conserved Cys residues in CTD, although the mechanistic basis for this inactivation remains unclear. For example, in the case of MutL from *Thermus thermophilus*, the replacement of one of the two conserved Cys in the CTD (C496A) led to the "turning off" of MMR *in vivo*, but the mutant form still retained the ability to hydrolyze plasmid DNA, which was comparable to the activity of the wild-type protein [14]. For human MutLα, it has also been shown that substitutions of C812S or C843S (at least one of the conserved Cys residues to serine) result in almost complete inactivation of MMR *in vitro* [15].

Cys residues are of particular interest as potential determinants of MutL function. Cys are frequently found in metal-coordinating motifs—such as zinc fingers and binuclear metal centers—where they contribute to the geometry of the catalytic site [16]. Given that the CTD of ngMutL harbors a metal-binding motif and that endonuclease activity requires divalent cations, the question of whether conserved Cys residues participate in metal ion coordination was of practical interest.

In particular, the CTD of ngMutL contains five Cys residues, two of which, C604 and C635, are conserved and located in the vicinity of the active site, whose roles in metal ion coordination and catalysis have not been fully elucidated. Whether these residues contribute to catalysis, metal ion coordination, or productive interaction with the sliding clamp remained an open question.

In the present study, we performed a comprehensive biochemical and biophysical characterization of wild-type ngMutL (ngMutL^{wt}) and a Cys-free variant (ngMutL^{cf}), in which all five Cys were replaced with evolutionarily conserved amino acids. Using experimental approaches and molecular dynamics simulations, we demonstrate for the first time that Cys residues are critical for efficient hydrolysis of linear DNA substrates in the presence of the DNA polymerase III β-subunit by maintaining the conformational rigidity of the CTD required for productive positioning of the catalytic domain relative to the sliding clamp.

2. Materials and Methods

2.1 Plasmids and Oligonucleotides

Plasmid pUC-MMR was used as a supercoiled substrate for endonuclease assays on plasmid DNA. Oligodeoxyribonucleotides were synthesized by standard phosphoramidite chemistry and purified by HPLC (Syntol, Russia). The ds76_TAMRA was prepared by annealing the TAMRA-labeled upper strand (3′-TAMRA) with a fully complementary unlabeled strand (used at a 5% molar excess) in 20 mM HEPES-KOH (pH 8.0), 100 mM KCl by heating to 95 °C for 5 min followed by slow cooling to room temperature. Oligonucleotide concentrations were determined spectrophotometrically using extinction coefficients calculated from nearest-neighbor data (https://www.idtdna.com/calc/analyzer).

2.2 Expression and Purification of Recombinant Proteins

The Cys-free variant ngMutL^{cf} was designed by replacing all five Cys residues with evolutionarily conserved substitutes (C171I, C251L, C532A, C604S, C635S), selected on the basis of large-scale multiple sequence alignment of bacterial MutL homologs. Wild-type ngMutL^{wt} and ngMutL^{cf} were expressed as N-terminal His$_6$-tagged

fusion proteins in *E. coli* BL21(DE3)Lys. Cells were grown in LB medium at 37 °C to OD_{600} ~0.6–0.8, induced with 1 mM IPTG, and cultured for an additional 3 h at 28 °C. Proteins were purified by Ni-NTA affinity chromatography followed by size-exclusion chromatography on a Superdex 200 10/300 column (GE Healthcare, Chicago, IL, USA) using an Äkta Purifier system (GE Healthcare, Chicago, IL, USA). Purified proteins were stored in 10 mM HEPES-KOH (pH 7.9), 300 mM KCl, 1 mM EDTA, 10% (v/v) glycerol, 1 mM 2-mercaptoethanol at −80 °C [12].

The β-subunit of DNA polymerase III (ngβ) was purified by Ni-NTA affinity chromatography followed by HiTrap Heparin HP (1 mL) chromatography pre-equilibrated in 10 mM K-phosphate buffer (pH 7.5) with 0.5 mM EDTA; the protein was eluted with a 0–0.5 M KCl gradient. The ngβ fractions were dialyzed into 10 mM HEPES-KOH (pH 7.9), 200 mM KCl, 1 mM EDTA, 10% (v/v) glycerol, aliquoted, and stored at −80 °C. Protein concentrations were determined spectrophotometrically at 280 nm using a NanoDrop ND-1000 (Thermo Fisher Scientific, Waltham, MA, USA); extinction coefficients were calculated with the ProtParam tool (https://web.expasy.org/protparam).

2.3 In Silico Residue Scanning and Mutational Analysis

To evaluate the thermodynamic effects of amino acid substitutions, in silico site-directed mutagenesis was performed using the Residue Scanning wizard within the BioLuminate module of the Schrödinger Suite (Schrödinger, LLC, New York, NY, USA). Each target residue was systematically substituted with the respective evolutionarily conserved or designated amino acid variants. Side-chain conformations of the mutated residues and neighboring residues within a cutoff radius of 5.0 Å were optimized using the Prime refinement algorithm. The changes in binding free energy ($\Delta\Delta G_{bind}$) and overall complex stability ($\Delta\Delta G_{stability}$) resulting from the mutations were calculated using the MM-GBSA (Molecular Mechanics-Generalized Born Surface Area) continuum solvation model.

2.4 Circular Dichroism Spectroscopy

CD spectra of ngMutL^{wt} and ngMutL^{cf} were recorded for the first time for full-length ngMutL. Protein samples (0.2–0.5 mg/mL) were measured in 10 mM sodium phosphate buffer (pH 7.5) on a Chirascan CD spectrometer (Applied Photophysics Ltd., Leatherhead, UK) in a 1 mm quartz cuvette over the wavelength range 200–260 nm at 25 °C. All CD spectra were baseline-corrected for buffer contributions and processed with the Origin 2018b software (version 9.55, OriginLab Corporation, Northampton, MA, USA) using the Savitzky–Golay filter.

2.5 ATPase Activity Assay

ATPase activity was measured colorimetrically using the malachite green phosphate detection reagent to quantify released inorganic phosphate. A calibration curve was constructed by measuring the absorbance of solutions containing known concentrations of inorganic phosphate (0–40 µM); the curve was linear over this range. Reaction mixtures (50 µL) contained 20 mM HEPES-KOH (pH 8.0), 100 mM KCl, 5 mM $MgCl_2$, 0.5 mg/mL BSA, 0.5 µM ngMutL^{wt} and ngMutL^{cf} (per dimer), 50 nM ds76, and ATP at concentrations ranging from 100 to 1000 µM. Reactions were incubated at 37 °C and quenched at defined time points by addition of malachite green reagent. The slope of the linear portion of each phosphate accumulation curve represents the initial reaction rate (v_0), values were expressed as µM Pi per minute and normalized to the molar concentration of the protein dimer to yield k_{cat} (min^{-1}). The dependence of v_0 on ATP concentration was fitted to the Michaelis–Menten equation by nonlinear regression using Origin 2018b (version 9.55, OriginLab Corporation, Northampton, MA, USA) to obtain K_M and V_{max}. All experiments were performed in triplicate.

$$E + S \leftrightarrow ES \rightarrow E + P$$

$$\nu = \frac{V_{max} * S}{S + K_M}$$

$$V_{max} = E_0 * k_{cat}$$

$$K_M = \frac{k_{-1} + k_2}{k_1}$$

2.6 DNA-Binding Assay (EMSA)

ds76_TAMRA (20 nM) was incubated with increasing concentrations of ngMutL^{wt} or ngMutL^{cf} (0–1600 nM per dimer) for 10 min on ice in 20 mM HEPES (pH 8.0), 100 mM KCl, 0.5 mg/mL BSA, 1 mM DTT. Samples (10–20 µL) were resolved by electrophoresis in a non-denaturing 6% polyacrylamide gel in TAE buffer at 4 °C for 2–3 h. Gels were visualized using a Typhoon FLA 9500 imager (GE Healthcare, Chicago, IL, USA) and quantified with TotalLab TL120 software (Nonlinear Dynamics Ltd., New Castle, UK). The extent of binding was calculated as the ratio of the fluorescence intensity of the protein–DNA complex band to total DNA fluorescence intensity. Apparent dissociation constants (K_d^{app}) and Hill coefficients (h) were determined by fitting binding curves to the Hill equation by nonlinear regression in Origin 2018b (version 9.55, OriginLab Corporation, Northampton, MA, USA). All experiments were performed in at least triplicate.

$$hE + L \rightarrow E_hL$$

$$E_t = E + EL$$

$$L_t = L + EL$$

$$K_d = \frac{E * L}{EL}$$

$$Y = \frac{Y_{max} * E^h}{(E^h + K_d^h)}$$

2.7 Endonuclease Activity on Plasmid DNA

Endonuclease activity on supercoiled DNA was assessed using plasmid pUC-MMR, monitoring conversion of the supercoiled form to the nicked open circular form by agarose gel electrophoresis. Reaction mixtures (20 µL) contained 20 mM HEPES-KOH (pH 8.0), 100 mM KCl, 5 mM $MnCl_2$, 0.5 mg/mL BSA, 0.5 nM plasmid, and 0.2–0.8 µM ngMutL^{wt} or ngMutL^{cf} (per dimer). Reactions were incubated at 37 °C for 0–60 min, except for the time-dependent hydrolysis experiment, for which the incubation time was extended to 150 min. Reactions were quenched by addition of 25 mM EDTA and 0.5% SDS. Products were analyzed by electrophoresis in 1% agarose gels stained with ethidium bromide and visualized under UV light.

2.8 Endonuclease Activity on Linear DNA Substrates

Endonuclease activity on linear substrates was assessed using ds76_TAMRA. The effects of divalent metal ions and ATP concentration were evaluated systematically. Reaction mixtures (10 µL) contained 20 mM HEPES-KOH (pH 8.0), 100 mM KCl, 0.5 mg/mL BSA, 12% (v/v) glycerol, 10 nM labeled duplex. For comparative experiments with ngMutL^{wt} and ngMutL^{cf}, optimized conditions were used: 5 mM $MgCl_2$, 5 mM $MnCl_2$, 0.5 mM ATP, 0.75 µM protein (per dimer), and an equimolar amount of ngβ dimer. Reactions were incubated at 37 °C for 90 min and quenched by addition of 50 mM EDTA and 1 mg/mL proteinase K, followed by incubation at 55 °C for 20 min. Products were resolved by denaturing PAGE (10% polyacrylamide, 7 M urea), visualized using a Typhoon FLA 9500, and quantified with TotalLab TL120. The hydrolysis efficiency was calculated as the ratio of the sum of cleavage product intensities to the total lane intensity.

2.9 Molecular Dynamics Simulations

The crystal structure of the *N. gonorrhoeae* MutL C-terminal domain in complex with the β-clamp (CTD-ngMutL:ngβ, PDB: 8XLA) was used as the starting model for all computational analyses. The cysteine-free variant of CTD-ngMutL was generated by introducing substitutions C532A, C604S, and C635S into chains Z and D of the wild-type structure using the Mutagenesis Wizard in PyMOL. ANISOU records were removed and residues with negative sequence numbers were renumbered prior to further processing. Production MD simulations were performed for 1.2 ns with an integration time step of 2 fs. The final frame of the trajectory was extracted as a representative frame for structural analysis.

All molecular dynamics simulations were carried out using the Desmond module with the OPLS4 force field. The initial protein-protein complexes (the top 10 poses for both variants) were solvated in an orthorhombic box filled with explicit SPC or TIP3P water molecules, maintaining a minimum buffer distance of 10 Å from the protein solute to the periodic boundary faces. The systems were neutralized by adding counterions (K^+ or Cl^-).

Prior to production runs, all systems were subjected to the default Desmond relaxation protocol, which included a series of minimized and short restrained simulations under both NVT and NPT ensembles. Production MD simulations were performed in the NPT ensemble at a constant temperature of 310 K (37 °C, matching the experimental assay temperature).

Intermolecular contacts at the CTD-ngMutL:ngβ interface were defined as residue pairs with at least one interatomic distance within 4 Å, and were analyzed for both the crystal structure and the MD-refined complexes. For structural comparison, the MD-refined wild-type and cysteine-free complexes were superimposed using the β-clamp dimer (chains A and B) as a reference frame in PyMOL. Distances between corresponding Cα atoms of the catalytic residues D491, H493, and E497 in the two variants were measured using the distance function in PyMOL. Molecular graphics were prepared using PyMOL.

2.10 Statistical Analysis

Each experiment was performed in three independent replicates. Data are presented as mean values with 95% confidence intervals or mean ± standard deviations, as indicated in the figures legends. Statistical comparisons between groups were performed using a two-tailed Student's *t*-test. A p-value < 0.05 was considered statistically significant. Statistical analysis was performed using Origin 2018b (version 9.55, OriginLab Corporation, Northampton, MA, USA).

3. Results

3.1 Purification and Secondary Structure of ngMutL^{wt} and ngMutL^{cf}

Since ngMutL contains five Cys residues (C171, C251, C532, C604, C635) whose individual and common contributions to protein function were unknown, we chose to generate a fully Cys-free variant as a defined baseline. This approach serves two purposes: first, it allows us to estimate the collective role of Cys residues without the interpretational ambiguity inherent to individual substitutions, where compensatory effects between residues cannot be excluded; second, a biochemically characterized Cys-free variant provides a clean scaffold for future studies in which selected Cys residues can be reintroduced at defined positions—for example, for site-specific fluorescent labeling or cross-linking experiments. The viability of this approach depends critically on whether the Cys-free variant retains the functional properties of the wild-type protein, which was the primary question addressed in the present study [17,18].

To investigate the functional role of Cys in ngMutL, we expressed and purified wild-type ngMutL^{wt} and a Cys-free variant (ngMutL^{cf}) in which all five Cys residues were replaced with evolutionarily conserved substitutes (C171I, C251L, C532A, C604S, C635S; Fig. 1). The substitutions were selected based on a large-scale comparison of MutL homolog sequences [19,20]. Based on this analysis, positions C171, C251 and C532 were shown to be located in the non-conservative MutL regions, and different amino acids are found in these positions. Ile, Leu and Ala were selected as the most common amino acids in similar positions in MutL proteins from other organisms (Ile171, Leu251 and Ala532 are found in 40%, 30% and 33% of analyzed sequences, respectively). While the two conserved Cys near the active site (C604 and C635) were replaced with serine [19,20].

Serine was chosen as the replacement for the two conserved cysteines near the active site (C604 and C635), rather than the more commonly used alanine, because serine most closely mimics the size and polarity of Cys while eliminating the reactive thiol group. To validate this choice computationally, we performed *in silico* mutational scanning within the BioLuminate framework, which confirmed that the substitutions in the CTD are structurally non-disruptive: the combination C532A, C604S, C635S yielded a net stabilizing free energy change (ΔStability = −6.22 kcal/mol) with a favorable increase in solvent-accessible polar surface area (ΔSASA polar = +178.31 Å^2), consistent with productive hydration of the introduced serine hydroxyl groups.

Both proteins were purified by Ni-NTA affinity chromatography followed by size-exclusion chromatography as described [12] yielding preparations with an apparent molecular weight of ~72 kDa, consistent with the calculated mass of the MutL monomer (**Supplementary Fig. 1**). To assess whether the Cys substitutions affected the overall fold of ngMutL^{cf}, we recorded CD spectra for both proteins. CD spectra of ngMutL^{wt} and ngMutL^{cf} were highly similar, exhibiting two characteristic minima at 208 nm and 222 nm, which is typical for proteins with a predominantly α-helical secondary structure (Fig. 2). These results indicate that the replacement of all Cys residues does not significantly alter the secondary structure of ngMutL, validating the use of ngMutL^{cf} in subsequent comparative experiments.

3.2 Cys Substitutions Do Not Impair DNA Binding and ATPase Activities

MutL homologs bind DNA non-specifically through the N-terminal domain, and binding efficiency is largely dependent on DNA length. Previously we have shown that ngMutL efficiently forms complexes with DNA fragments longer than 40–41 bp, with apparent dissociation constants in the nanomolar range both for duplex and G4-containing substrates [7]. Binding affinity was found to depend on DNA length, topology, and ionic conditions: for duplex substrates of 41 and 95 bp, K_d^{app} values of 650 ± 85 and 123 ± 8 nM were determined, respectively, while for G4-containing single-stranded oligonucleotides of the same lengths, affinities were markedly higher (135 ± 30 and 41 ± 1 nM, respectively), reflecting the preferential recognition of noncanonical DNA structures by ngMutL [7]. These results are consistent with published data on MutL homologs from other species and confirm that ngMutL DNA-binding activity is a robust, length and structure sensitive property of the protein. We compared the DNA-binding capacities of ngMutL^{wt} and ngMutL^{cf} using electrophoretic mobility shift assay (EMSA; **Supplementary Fig. 2A,B**) with the 76-bp DNA-duplex carrying a TAMRA fluorophore at the 3′-end of the upper strand (ds76_TAMRA):

5′-ATAGGACGCTGACACTGGTGCTTGGCAGC TGAGCCATATGCTCGAGTAACGCTCATAGGATCC AAGCGCGAAAGGA-3′-TAMRA

3′-TATCCTGCGACTGTGACCACGAACCGTCG ACTCGGTATACGAGCTCATTGCGAGTATCCTAGG TTCGCGCTTTCCT-5′

At 100 mM KCl, ngMutL^{cf} reached nearly complete binding (≥95%) at protein concentrations of 0.75–1 μM, comparable to ngMutL^{wt}. Apparent dissociation constants determined using the Hill model were identical within experimental error for both variants (K_d^{app} = 117 ± 7 nM for ngMutL^{wt} and 118 ± 6 nM for ngMutL^{cf}; Hill coefficient ~3.0) (Table 1). These results indicate that Cys residues are not involved in direct contacts with the DNA substrate.

Table 1. Apparent dissociation constants for ngMutL^{wt} and ngMutL^{cf} binding to ds76_TAMRA.

Protein	K_d^{app}, nM	Hill coefficient
ngMutL^{wt}	117 ± 7	2.9 ± 0.2
ngMutL^{cf}	118 ± 6	3.1 ± 0.4

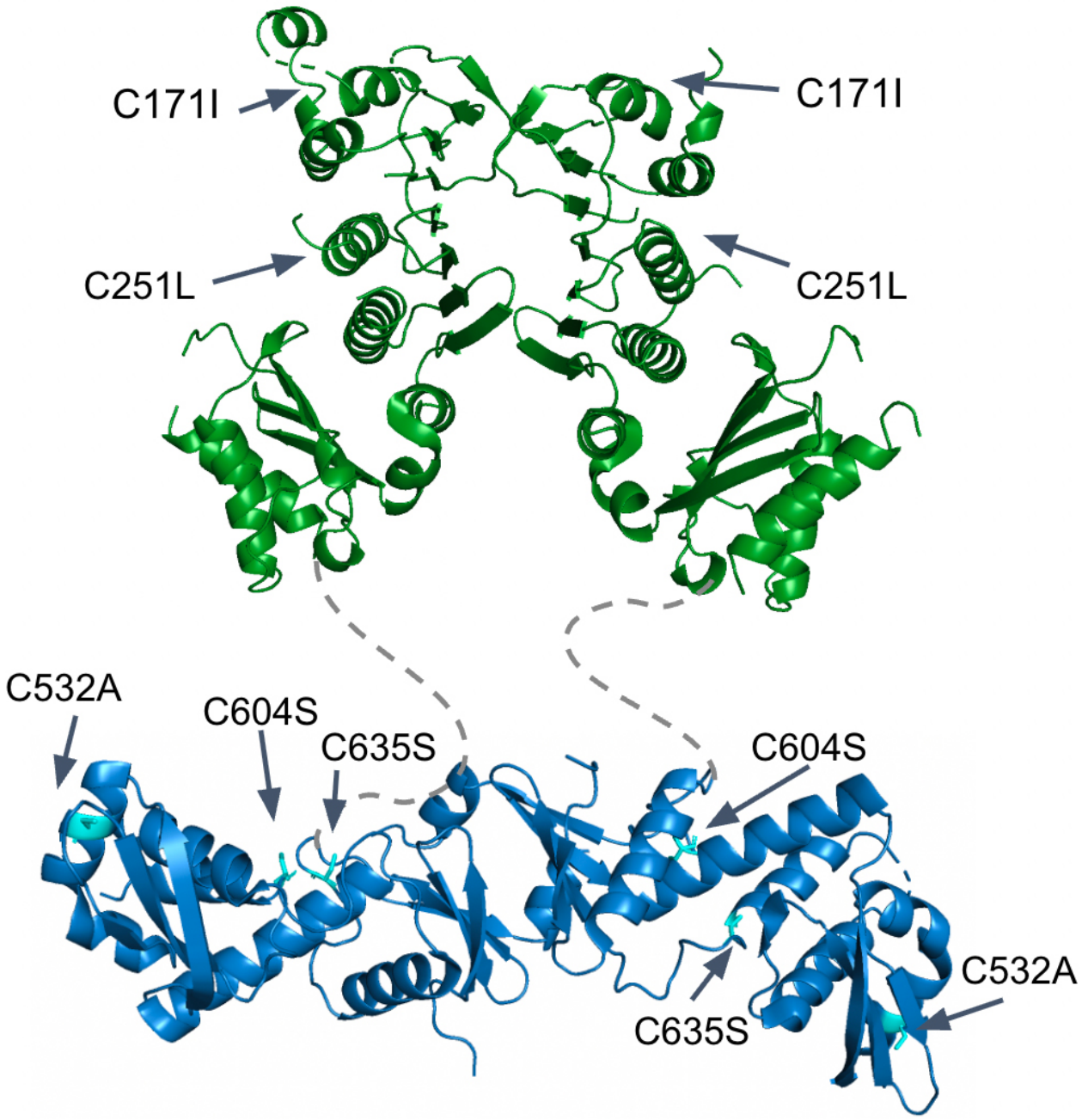

Fig. 1. Schematic representation of the ngMutL^{cf} protein, in which all cysteine residues were substituted with alternative amino acid residues. The scheme is based on the PDB: 1BKN, 3NCV. N-terminal domain and C-terminal domain are shown green and blue, respectively.

ATP binding and hydrolysis in the ATPase center of MutL drive conformational changes required for interaction with other MMR components and activation of endonuclease activity [21]. ATPase activity of both proteins was assessed colorimetrically using malachite green dye in the presence of ds76_TAMRA, which was previously shown to stimulate ATP hydrolysis by ngMutL [12]. A calibration curve was obtained by measuring the absorbance of solutions containing predetermined concentrations of inorganic phosphate, and was used to calculate the phosphate concentration in the experimental samples. The time-dependent accumulation of inorganic phosphate produced during ATP hydrolysis by ngMutL^{wt} and ngMutL^{cf} at various substrate concentrations is presented in **Supplementary Fig. 3A,B**. The slope of the linear portion of each time course represents the initial reaction rate (v_0). The dependences of the initial ATP hydrolysis rate (v_0) on ATP concentration for both ngMutL^{wt} and ngMutL^{cf} are shown in **Supplementary Fig. 3C**. Kinetic parameters of the ATP hydrolysis for both proteins were determined by nonlinear regression using the

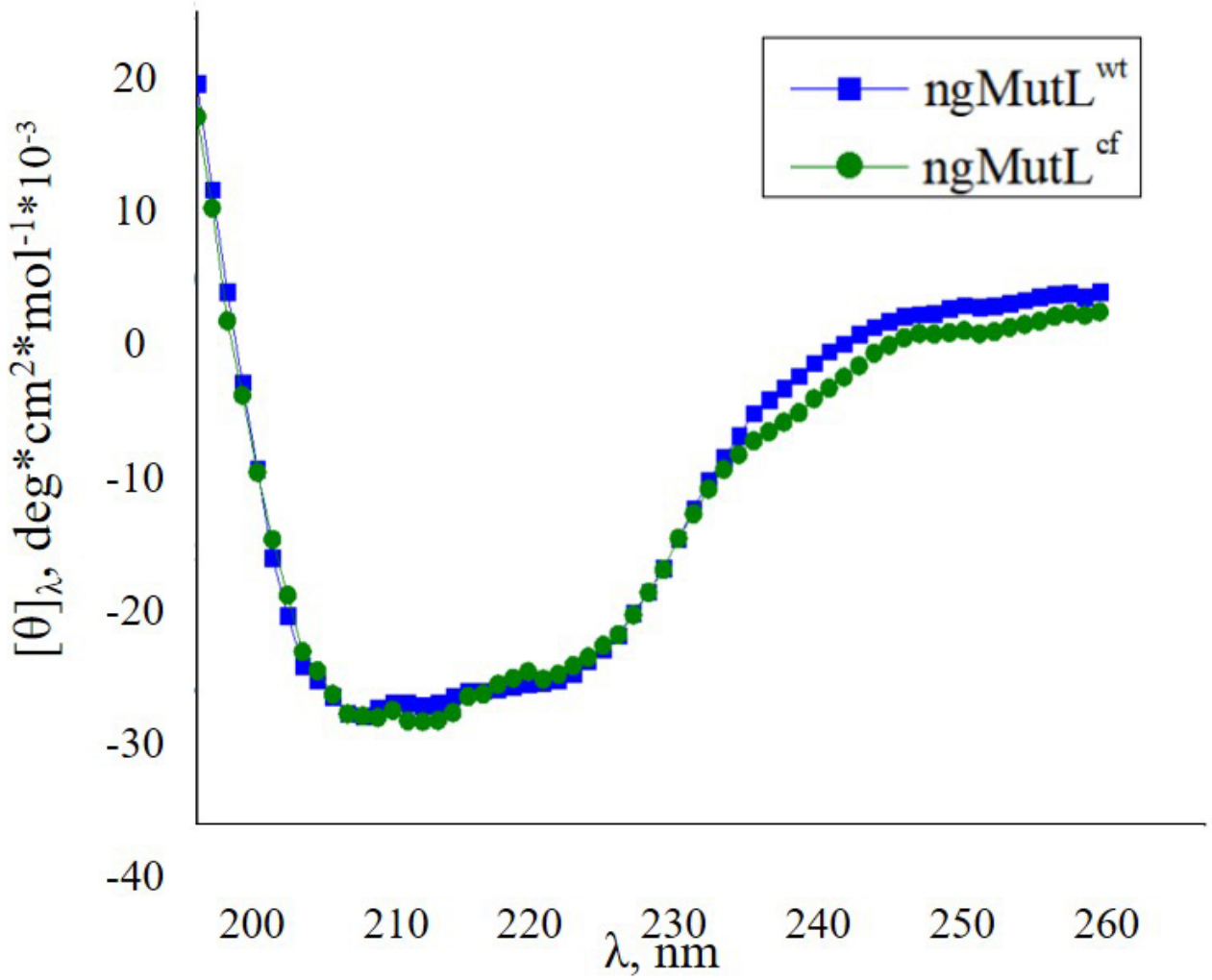

Fig. 2. CD spectra of ngMutL^{wt} (blue) and ngMutL^{cf} (green). Spectra were recorded at 25 °C in 10 mM sodium phosphate buffer (pH 7.5) over the 200–260 nm range, using a protein concentration of 0.2–0.5 mg/mL in a 0.1-cm path-length cuvette.

Michaelis–Menten equation implemented in Origin 2018b (version 9.55) and are summarized in Table 2. The apparent affinity for ATP was identical within experimental error for both variants (K_M = 377 ± 16 μM for ngMutL^{wt} and 354 ± 16 μM for ngMutL^{cf}), indicating that Cys substitutions do not affect substrate binding. However, the maximum hydrolysis rate (V_{max}) was reduced by approximately 20% in ngMutL^{cf} compared to ngMutL^{wt} (0.36 ± 0.01 or 0.285 ± 0.005 μM*min^{-1}, respectively). Thus, although Cys residues do not participate in ATP binding, they nevertheless contribute slightly to the catalytic efficiency of the ATPase reaction.

Table 2. Kinetic parameters of ATP hydrolysis by ngMutL^{wt} and ngMutL^{cf}.

Protein	K_M, μM	V_{max}, μM*min^{-1}	k_{cat}, min^{-1}
ngMutL^{wt}	377 ± 16	0.36 ± 0.01	0.72 ± 0.01
ngMutL^{cf}	354 ± 16	0.285 ± 0.005	0.57 ± 0.01

3.3 Endonuclease Activity of ngMutL^{wt} and ngMutL^{cf} on Plasmid DNA

The endonuclease activity of ngMutL is localized in the C-terminal domain and requires divalent metal ions. Since MutL homologs lack mismatch specificity, substrates without mismatches were used in all hydrolysis assays. Endonuclease activity was first assessed using plasmid pUC-MMR as a substrate, monitoring conversion of the supercoiled form to the nicked (open circular) form by agarose gel electrophoresis (**Supplementary Fig. 4**).

Both ngMutL^{wt} and ngMutL^{cf} were capable of introducing single strand breaks into plasmid DNA in the presence of Mn^{2+}. After 60 min of incubation at 37 °C, the efficiency of plasmid hydrolysis was comparable between the two variants (Fig. 3).

Kinetic analysis revealed that ngMutL^{wt} initiated hydrolysis from the earliest time points, whereas ngMutL^{cf}

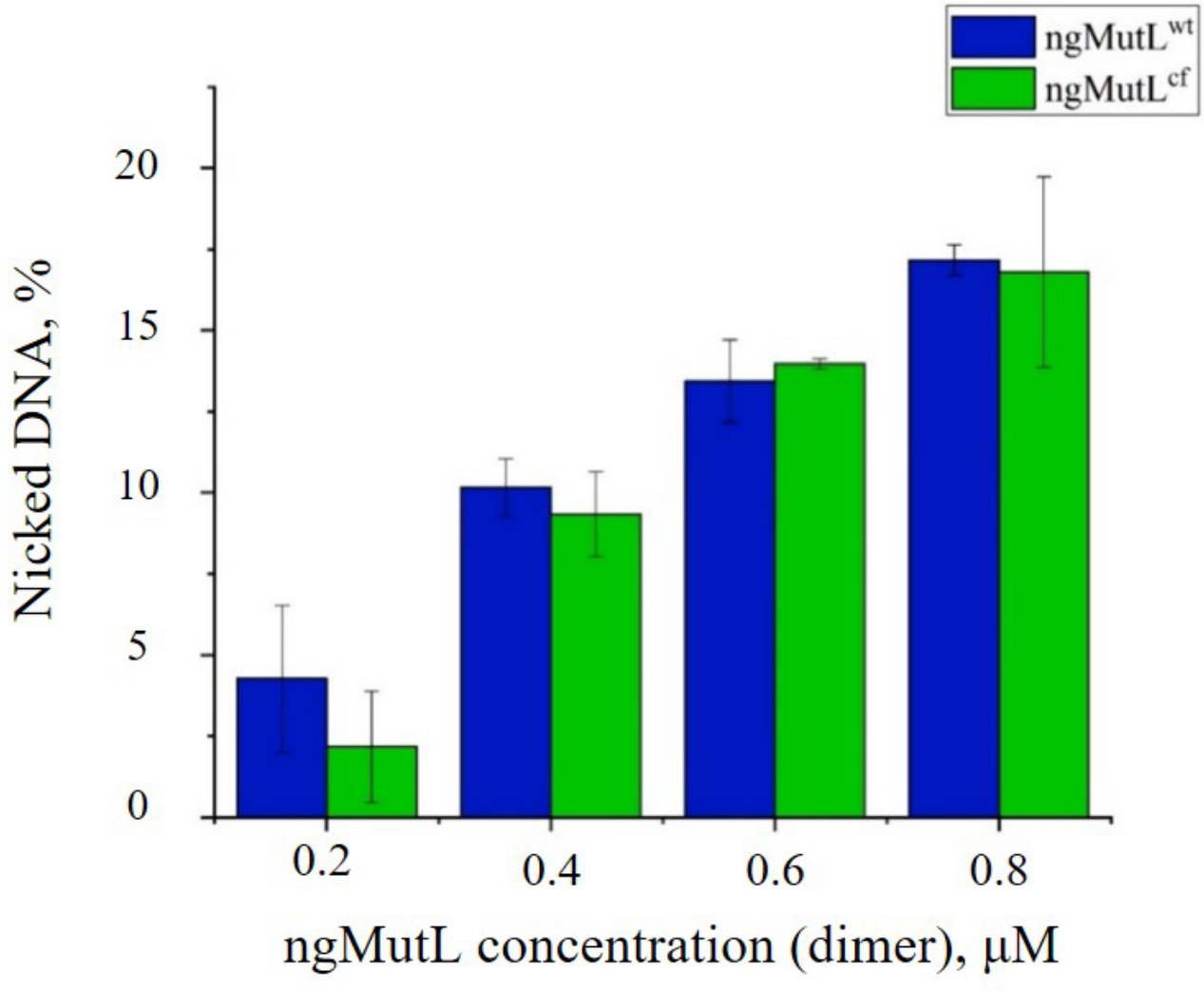

Fig. 3. Comparative analysis of pUC-MMR plasmid hydrolysis by ngMutL^{wt} and ngMutL^{cf} at 37 °C for 60 min. The percentage of nicked DNA formed during plasmid hydrolysis is shown. Error bars represent standard deviations. Differences were not statistically significant (Student's *t*-test, $p > 0.05$). The calculation was carried out for three independent experiments.

showed a lag phase of approximately 5 min; in the 10–30 min range, hydrolysis by ngMutL^{cf} was slightly less efficient, but by 60 min the difference was no longer significant (**Supplementary Fig. 5**). These results demonstrate that Cys substitutions do not substantially impair the endonuclease function of ngMutL on supercoiled plasmid substrates, and that the Cys residues are not essential for metal ion coordination or catalysis per se. Accordingly, ngMutL^{cf} was considered suitable for further comparative experiments.

3.4 Cys Residues Are Critical for ngMutL Endonuclease Activity on Linear Substrates in the Presence of the Sliding Clamp

Although endonuclease activity on supercoiled plasmid DNA provides a convenient readout of the intrinsic catalytic competence of ngMutL, this substrate does not reflect the topology of the physiological MMR target. In *N. gonorrhoeae*, as in other bacteria, mismatch repair operates on the chromosomal DNA in the vicinity of the replication fork, where the substrate is a linear duplex rather than a supercoiled molecule. Moreover, cleavage of plasmid DNA by MutL homologs does not require the β-clamp *in vitro*, whereas β-clamp-dependent nicking of linear substrates is thought to represent the mechanistically relevant pathway for strand discrimination during MMR *in vivo* [1,22,23,24]. Linear duplex substrates therefore impose a more stringent requirement on the protein: productive activity demands not only an intact catalytic center, but also sufficient DNA-binding affinity and, critically, a functional interaction with the sliding clamp. For these reasons, we next examined the endonuclease activity of ngMutL^{wt} and ngMutL^{cf} on linear DNA substrates.

The endonuclease activity of ngMutL on linear DNA substrates has been previously examined in our earlier stud-

ies [7,13]. We demonstrated that ngMutL, in the presence of the *N. gonorrhoeae* β-subunit of DNA polymerase III (ngβ), is capable of nicking linear duplex substrates in a strictly β-clamp-dependent manner. Notably, hydrolysis of the same ds76 linear duplex in the presence of ngβ yielded cleavage products of heterogeneous length ranging from short (~10 nt) to longer fragments (~30–50 nt), whose distribution varied with ATP concentration. This heterogeneity likely reflects ATP-dependent conformational dynamics of the full-length protein: unlike the isolated CTD, which requires a forked substrate geometry for productive cleavage [1], full-length ngMutL may promote local strand separation at the ends of linear duplexes through NTD-mediated remodeling, thereby generating the single-stranded substrate required for endonucleolytic cleavage by the CTD.

To assess the endonuclease activity ngMutL^{wt} and ngMutL^{cf} on linear substrates, we used ds76_TAMRA. In the present study, reaction conditions were optimized to achieve maximal endonuclease activity of ngMutL^{wt} on the linear substrate. Under the established conditions (750 nM ngMutL dimer, 10 nM ds76_TAMRA, 5 mM $MgCl_2$, 5 mM $MnCl_2$, 0.5 mM ATP, equimolar ngβ dimer, 37 °C, 90 min), ngMutL^{wt} achieved near-complete (≥95%) hydrolysis of the linear duplex, as evidenced by the virtual disappearance of the full-length substrate band and the appearance of short cleavage products on denaturing PAGE (Fig. 4). In the absence of ngβ, no hydrolysis of the linear substrate was detected regardless of metal ion composition, confirming the strict β-clamp dependence of ngMutL endonuclease activity on linear DNA.

Under the optimized conditions described above, we compared the endonuclease activity of ngMutL^{wt} and ngMutL^{cf} on the ds76_TAMRA. While ngMutL^{wt} efficiently hydrolyzed the substrate, the Cys-free variant showed drastically reduced activity, with hydrolysis not exceeding 15% regardless of ATP concentration (0–5 mM) (Figs. 5,6). This sharp decrease contrasts with the standard activity of ngMutL^{cf} on plasmid DNA, pointing to a specific effect in the β-clamp-dependent hydrolysis pathway rather than a general loss of catalytic competence.

Maximal hydrolysis of ds76 by ngMutL^{wt} was observed at concentrations of 0.5 mM, with 1–2 mM still showing relatively high activity (but not the peak), and a clear decrease at 3 and 5 mM (Fig. 6), likely due to chelation of the metal ions required for catalysis. This effect was previously described for DNA-binding activity of ngMutL [7]. Notably, for ngMutL^{cf}, hydrolysis remained consistently low across the entire range of ATP concentrations tested (0–5 mM), indicating that the reduced endonuclease activity of the Cys-free variant is independent of nucleotide cofactor concentration and reflects a structural rather than catalytic deficiency.

3.5 Cys Residues Maintain the Conformational Organization of the ngMutL–Sliding Clamp Complex

The molecular basis of strand discrimination in methylation-independent MMR was recently established by Nirwal et al. [1], who determined the crystal structure of the CTD-ngMutL:ngβ complex (PDB: 8XLA). The structure reveals that the CTD-ngMutL homodimer sits transversely across the C-terminal face of the β-clamp ring, with each CTD monomer engaging one monomer of the clamp through the conserved QHLLIP motif. This arrangement blocks the central DNA channel of the clamp, forcing the two strands of the duplex to separate: the newly synthesized daughter strand is directed towards the active site of one CTD monomer, while the parental template strand is diverted to a distal cavity, away from the active site of the second monomer. Strand discrimination is thus achieved through a structural strategy dependent on the precise geometry of the CTD-ngMutL:ngβ complex.

The CTD of ngMutL contains three Cys residues, of which two—C604 and C635—are conserved across bacterial MutL homologs and located in the vicinity of the endonuclease active site. To investigate whether these residues contribute to the conformational integrity of the CTD required for productive interaction with the sliding clamp, we used the crystal structure 8XLA as a starting model. The three Cys residues present in the CTD were replaced *in silico* with their evolutionarily conserved substitutes (C532A, C604S, C635S) to generate the CTD-MutL^{cf} model. Both the wild-type and Cys-free CTD structures were subjected to molecular dynamics simulations in explicit solvent to assess the effect of Cys substitutions on the stability of the CTD-ngMutL:ngβ interface.

Analysis of intermolecular contacts at the CTD-ngMutL:ngβ interface (defined as residue pairs within 4 Å, **Supplementary Tables 1,2**) revealed that in both variants the QHLLIP motif participates in binding to the hydrophobic pocket of the β-clamp, confirming that the overall binding mode is preserved (Fig. 7A,B).

In the crystal structure of the CTD-ngMutL:ngβ complex (PDB: 8XLA), the interface comprises 5 specific contacts mediated predominantly by the second CTD monomer (chain Z; Fig. 8).

Following MD simulation, the number of stabilizing specific contacts (h-bonds) in the wild-type complex increased, with the catalytically active monomer (chain D) forming additional hydrogen bonds with the clamp—consistent with the model proposed by Nirwal et al. [1] in which one CTD monomer is primarily responsible for directing the daughter strand towards the active site (Fig. 9).

Notably, residue L520 of the QHLLIP motif in the catalytically active monomer (chain D) forms a specific hydrogen bond with D239 of the β-clamp (chain B) in the wild-type complex, whereas in the Cys-free variant this contact is absent and L520 forms only van der Waals interactions with Y154 of chain B (**Supplementary Tables 1,2**). In contrast,

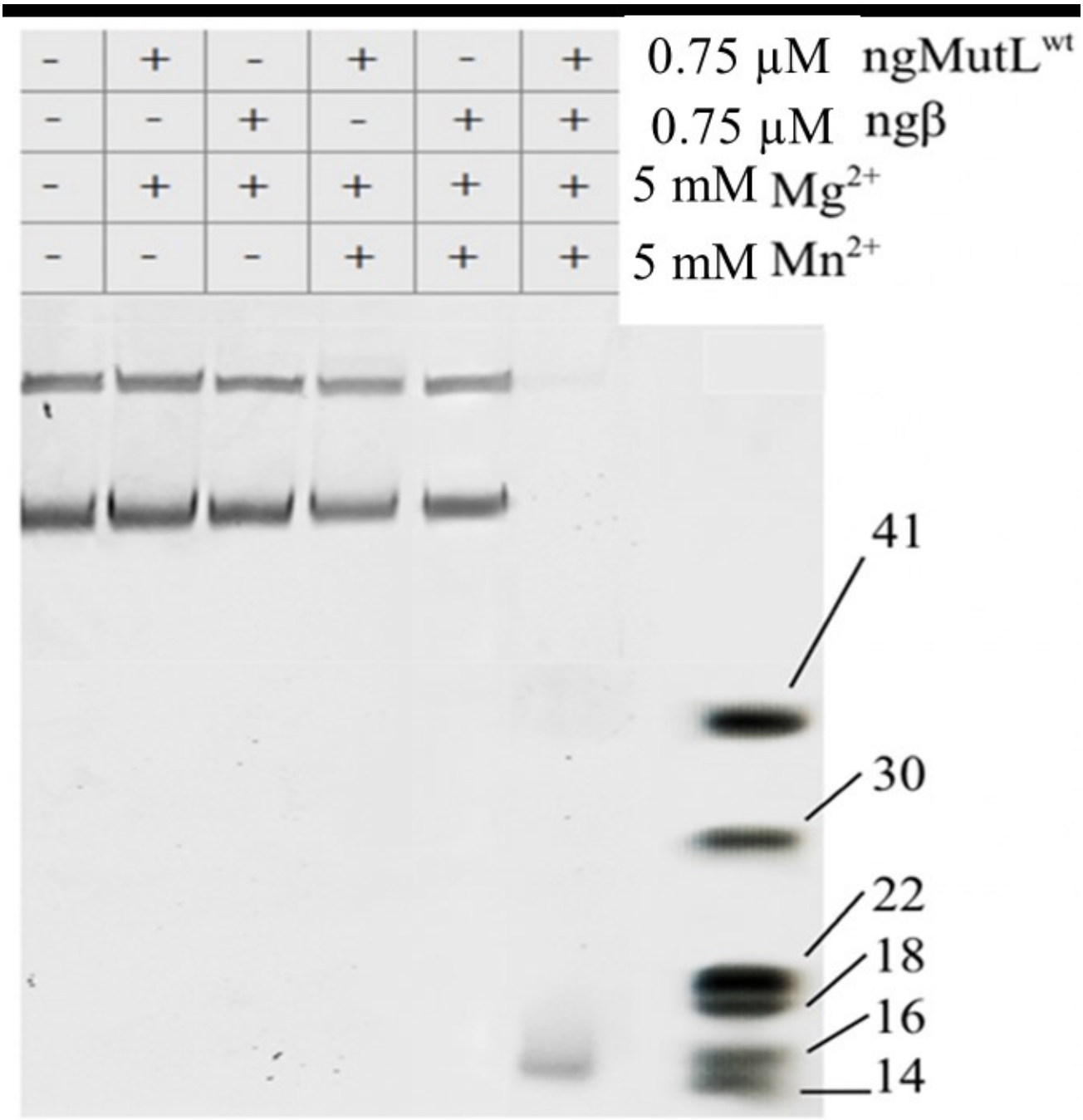

Fig. 4. Hydrolysis of ds76_TAMRA by ngMutL^{wt}. The reaction mixtures were incubated at 37 °C for 90 min. ngMutL^{wt} (0.75 μM) was used in the presence of an equimolar amount of ngβ dimer. $MgCl_2$, $MnCl_2$, ngMutL^{wt}, and ngβ were included in the reaction mixtures as indicated above each lane. Reaction products were analyzed by electrophoresis in 10% polyacrylamide gel containing 7 M urea in TBE buffer. The lengths of DNA markers, M (in nucleotide residues), are shown.

in the Cys-free variant after MD, the catalytically active monomer was involved in the formation of weaker van der Waals contacts with the clamp interface, all detectable hydrogen bonds confined to the second monomer (chain Z)—the one not predicted to engage the daughter strand in the strand discrimination model (Fig. 10).

To quantify this displacement, the MD-refined structures of the wild-type and Cys-free complexes were superimposed using the β-clamp dimer (chains A and B) as a reference. The catalytic residues D491, H493, and E497 of the active monomer were displaced by 17.0, 13.9, and 15.4 Å, respectively, in the Cys-free variant relative to the wild-type complex (Fig. 7B). This displacement—comparable in magnitude to the diameter of single-stranded DNA (~10 Å)—is sufficient to prevent productive positioning of the daughter strand within the active site, providing a struc-

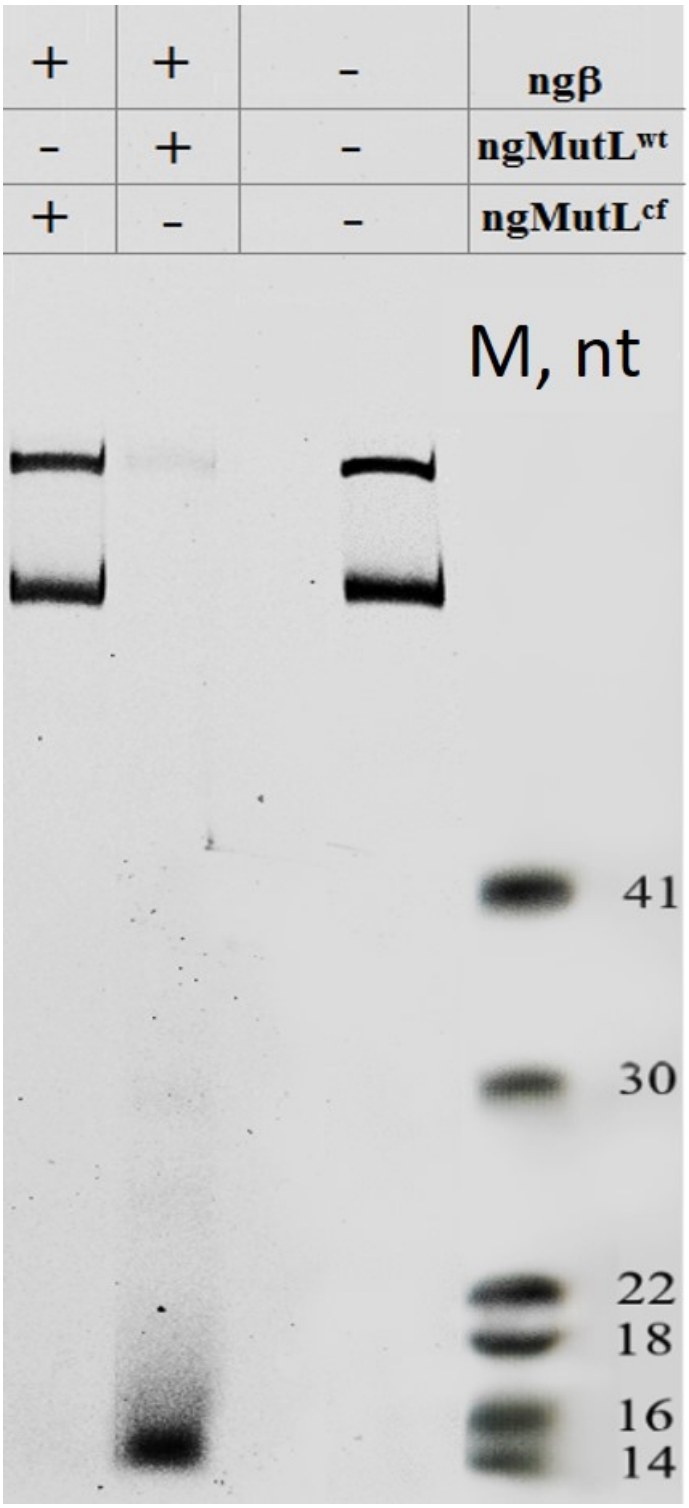

Fig. 5. Cleavage of ds76_TAMRA by ngMutL^{wt} and ngMutL^{cf}. The reaction mixtures were incubated in the presence 5 mM $MgCl_2$, 5 mM $MnCl_2$, and 0.5 mM ATP at 37 °C for 90 min. Proteins ngMutL^{wt} and ngMutL^{cf} (0.75 μM each) were used in the presence of an equimolar amount of ngβ dimer. Reaction products were analyzed by electrophoresis in a 10% polyacrylamide gel containing 7 M urea. Corresponding protein is present (+) or absent (-) in the incubation mixture. The lengths of DNA markers, M (in nucleotide residues), are shown.

tural explanation for the nearly complete loss of β-clamp-dependent endonuclease activity observed for ngMutL^{cf} on linear DNA substrates.

Taken together, these computational results demonstrate that although the Cys residues of ngMutL are not directly involved in ATP hydrolysis, DNA binding, or en-

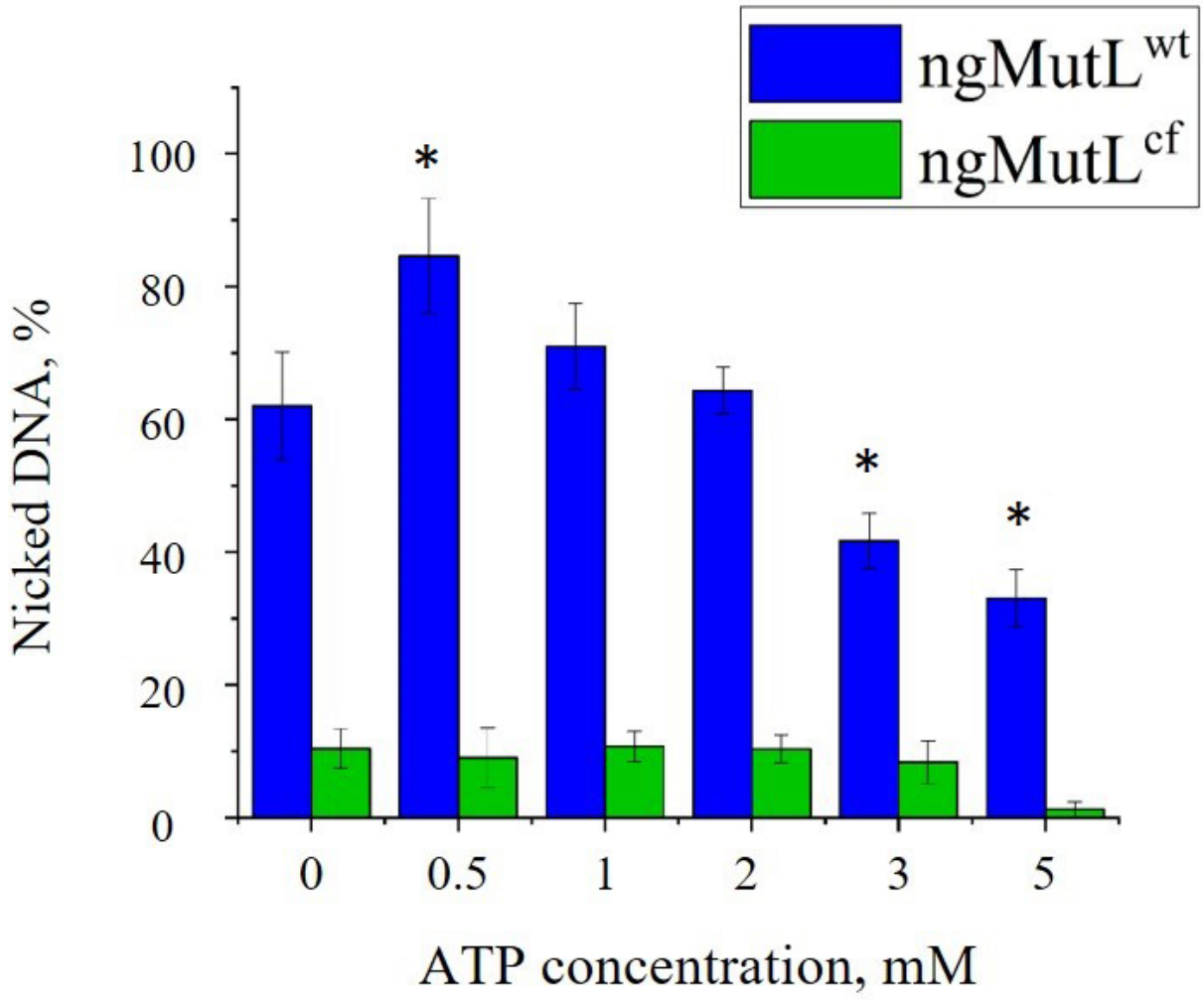

Fig. 6. ATP influence on ds76_TAMRA cleavage by ngMutL^{wt} and ngMutL^{cf}. The reaction mixtures were incubated in the presence of 0–5 mM ATP, 5 mM $MnCl_2$ for 90 min at 37 °C. Proteins ngMutL^{wt} and ngMutL^{cf} (0.75 μM each) were used in the presence of an equimolar amount of ngβ dimer. Reaction products were analyzed by electrophoresis in 10% polyacrylamide gel containing 7 M urea. Data are presented as mean ± SD from three independent experiments (n = 3). Statistical significance was assessed using Student's *t*-test by pairwise comparison of each ATP-containing condition (0.5–5 mM ATP) with the corresponding control without ATP (0 mM), separately for ngMutL^{wt} and ngMutL^{cf}. Differences were considered statistically significant at $p < 0.05$. Significant differences are indicated in the figure by asterisks (*$p < 0.05$); no significant differences were observed for ngMutL^{cf}.

donuclease catalysis, they are essential for maintaining the conformational rigidity of the C-terminal domain required for productive engagement with the sliding clamp. Their substitution alters the conformational organization of the MutL-ngβ complex in solution, impairing the geometric arrangement required for β-clamp-dependent endonuclease activity on linear DNA substrates.

4. Discussion

The present study provides a comprehensive biochemical and structural characterization of the role of Cys residues in *Neisseria gonorrhoeae* MutL, a key effector of the methyl-independent mismatch repair pathway. Using a Cys-free variant, ngMutL^{cf}, in which all five Cys residues were replaced with evolutionarily conserved substitutes, we demonstrate that these residues are dispensable for the overall protein fold, ATP hydrolysis, DNA binding, and endonuclease activity on supercoiled plasmid substrates, but are critically required for sliding clamp-dependent endonuclease activity on linear DNA duplexes. The highly similar CD spectra of ngMutL^{wt} and ngMutL^{cf} indicate that Cys substitutions do not cause major alterations in the global secondary structure of the protein. Thus, the strong reduction in linear DNA cleavage is unlikely to result from generalized protein unfolding or loss of the principal biochemical activities of ngMutL.

IMR Press

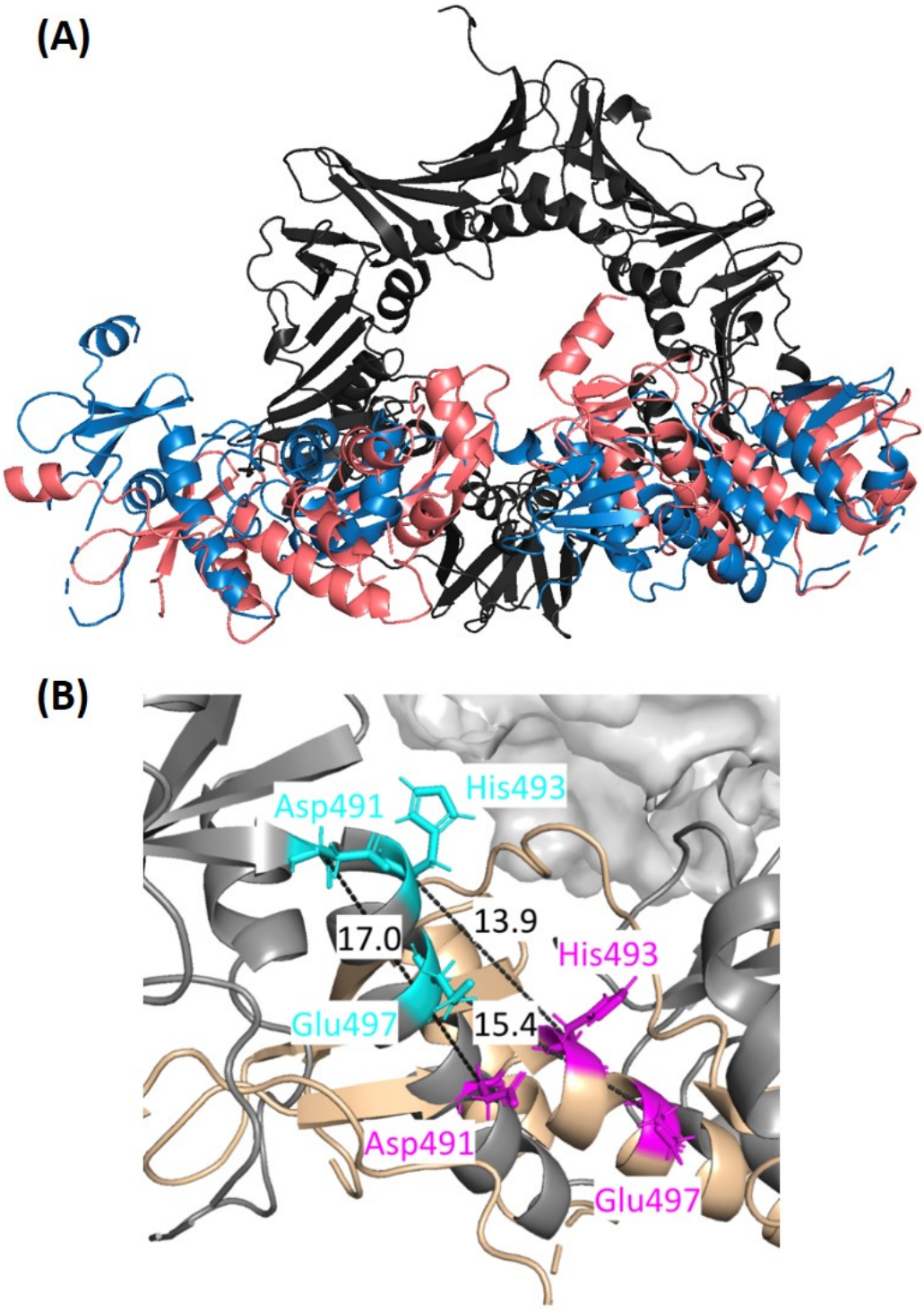

Fig. 7. Structural comparison of the wild-type and Cys-free CTD-ngMutL:ngβ complexes after molecular dynamics simulation. (A) Superposition of the MD-refined wild-type (blue) and Cys-free (red) CTD-ngMutL dimers after alignment on the β-clamp dimer (black). (B) Close-up view of the catalytic active site residues D(Asp)491, H(His)493, and E(Glu)497 in the wild-type (cyan) and Cys-free (magenta) variants after alignment on the β-clamp (grey surface). Black dashed lines indicate distances between corresponding Cα atoms.

The most informative observation is the contrasting behavior of ngMutL^{cf} on supercoiled plasmid and linear DNA substrates. The Cys-free protein retained the ability to nick supercoiled plasmid DNA, indicating that its endonuclease center remained catalytically competent under conditions in which cleavage did not require the sliding clamp.

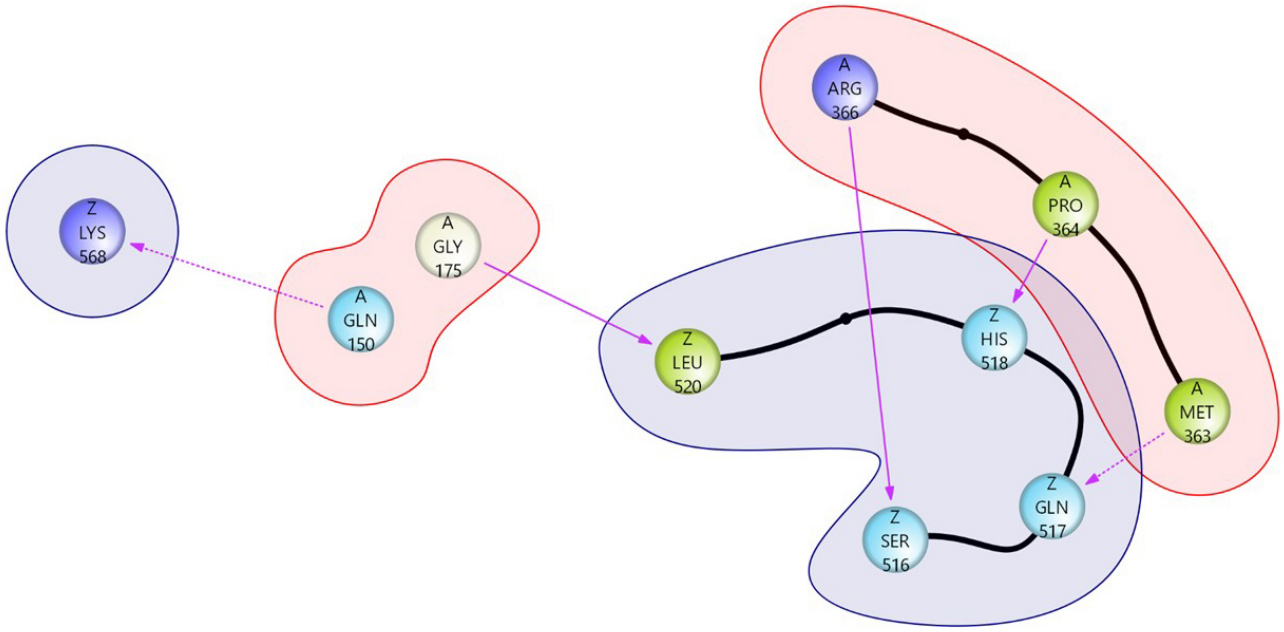

Fig. 8. 2D interaction maps of the CTD-ngMutL:ngβ interface. The initial interaction network based on the wild-type crystal structure (PDB: 8XLA) prior to molecular dynamics (MD) simulation, showing contacts mediated predominantly by the second CTD monomer (chain Z). Chain A (β-clamp monomer 1) is shown in red, chain Z (CTD monomer 1, non-catalytic) in purple. Magenta solid and dotted arrows indicate hydrogen bonds involving backbone and side-chain atoms, respectively, pointing from the hydrogen bond donor to the acceptor.

In contrast, ngMutL^{cf} displayed only minimal activity on the linear duplex, whose cleavage was strictly dependent on ngβ. This functional difference suggests that the substitutions do not abolish endonuclease activity per se, but interfere with a requirement that becomes critical specifically during β-clamp-dependent cleavage.

This distinction is relevant to the mechanism of methyl-independent MMR. In these systems, the sliding clamp does more than recruit MutL to DNA. The recently determined structure of the ngMutL CTD–ngβ complex indicates that strand discrimination depends on a specific spatial arrangement in which the MutL CTD is positioned across the clamp and one DNA strand is directed toward the endonuclease active site [1]. Consequently, the presence of an intact catalytic center and measurable interaction with the sliding clamp may not be sufficient for cleavage. The complex must also adopt a geometry that allows the daughter strand to reach the catalytic site in a productive orientation.

Several explanations could in principle account for the loss of activity of ngMutL^{cf} on the linear substrate. Cys substitution might weaken the interaction with ngβ, impair assembly of the complex on DNA, alter the relative orientation of MutL and the clamp, or affect conformational transitions required after complex formation. However, EMSA (**Supplementary Fig. 6**), biolayer interferometry and BS3-mediated cross-linking (data not shown) did not reveal detectable differences between ngMutL^{wt} and ngMutL^{cf} in their interaction with ngβ. Although these experiments cannot exclude subtle changes in affinity, kinetics, or transient DNA-associated states, they argue against a substantial loss of β-clamp binding as the principal cause of inactivation.

The molecular dynamics simulations suggest an alternative explanation. In both simulated complexes, the principal β-clamp-binding motif remained associated with the clamp, indicating preservation of the general interaction mode. At the same time, the Cys-free CTD adopted a different orientation relative to ngβ, and the catalytically active monomer was displaced from the position observed in the wild-type model. Such a rearrangement could prevent productive delivery of the DNA strand to the active site without necessarily causing dissociation of MutL from the clamp. Thus, the simulations support a model in which the loss of activity results from altered conformational organization of the ngMutL–ngβ complex rather than from disruption of complex formation itself.

This interpretation should nevertheless be regarded as a mechanistic hypothesis rather than direct structural proof. The simulations were relatively short, were initiated from a single crystallographic conformation, and did not include DNA or catalytic metal ions. Moreover, the experimental assays used here do not directly monitor the orientation of the CTD within the DNA-bound complex. Longer simulations, preferably including DNA and divalent cations, together with structural or single-molecule approaches, will be required to determine whether the con-

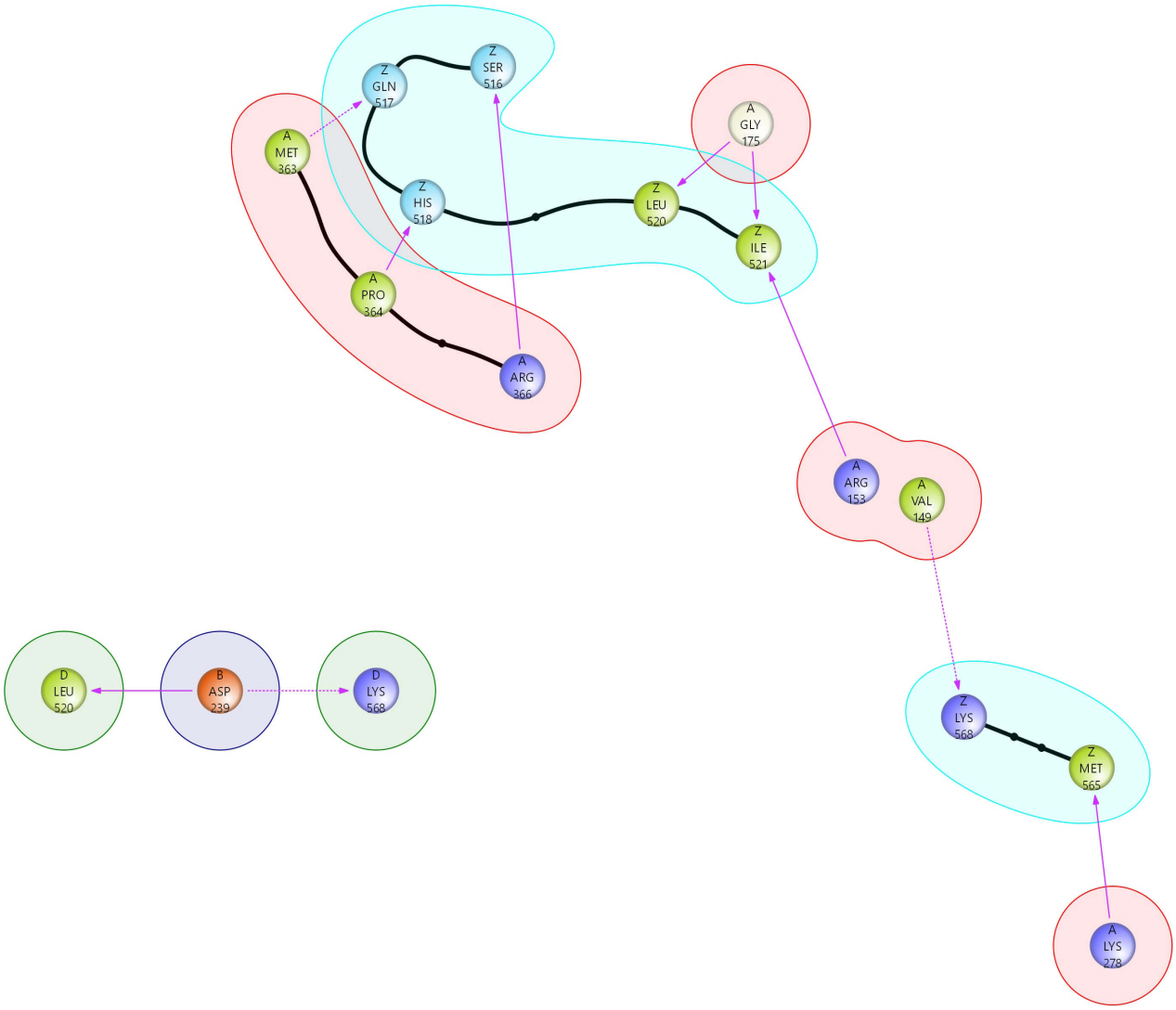

Fig. 9. 2D interaction maps of the CTD-ngMutL:ngβ interface after MD simulation. The interface is stabilized by an increased number of hydrogen bonds, crucially including the engagement of the catalytically active CTD monomer (chain D, shown in green) with the β-clamp (chain B, purple). Chain A (β-clamp monomer 1) is shown in red, Chain B (β-clamp monomer 2) is shown in purple, chain Z (CTD monomer 1, non-catalytic) in blue, chain D (CTD monomer 2, catalytic) in green. Magenta solid and dotted arrows indicate hydrogen bonds involving backbone and side-chain atoms, respectively, pointing from the hydrogen bond donor to the acceptor.

formational displacement observed *in silico* occurs during β-clamp-dependent cleavage.

Previous studies have shown that substitution of Cys residues in bacterial MutL homologues and human MutLα can strongly reduce MMR activity, while in some cases intrinsic endonuclease activity on model substrates is retained [14,15]. The present findings are consistent with these observations and suggest why assays based solely on plasmid nicking may not fully reflect the functional state of MutL in methyl-independent MMR. A protein may retain an active endonuclease center yet fail to cleave DNA in the strand-discrimination complex if the catalytic domain is not positioned correctly relative to the sliding clamp and the DNA substrate.

Finally, the Cys-free variant characterized in this study may itself serve as a valuable tool for investigating the non-canonical properties of ngMutL. We have previously shown that ngMutL displays enhanced binding affinity for G-quadruplex structures, including the *pilE* G4 located upstream of the pilin promoter, yet does not hydrolyze DNA within the quadruplex core—suggesting a role for ngMutL in the regulation of pilin antigenic variation that is independent of its endonuclease function [7]. Since ngMutL^{cf} retains ATPase activity, DNA-binding capacity, and endonuclease activity on plasmid substrates, but is specifically deficient in sliding clamp-dependent hydrolysis of linear DNA, it provides a means to study such DNA recognition events in the absence of productive endonucleolytic pro-

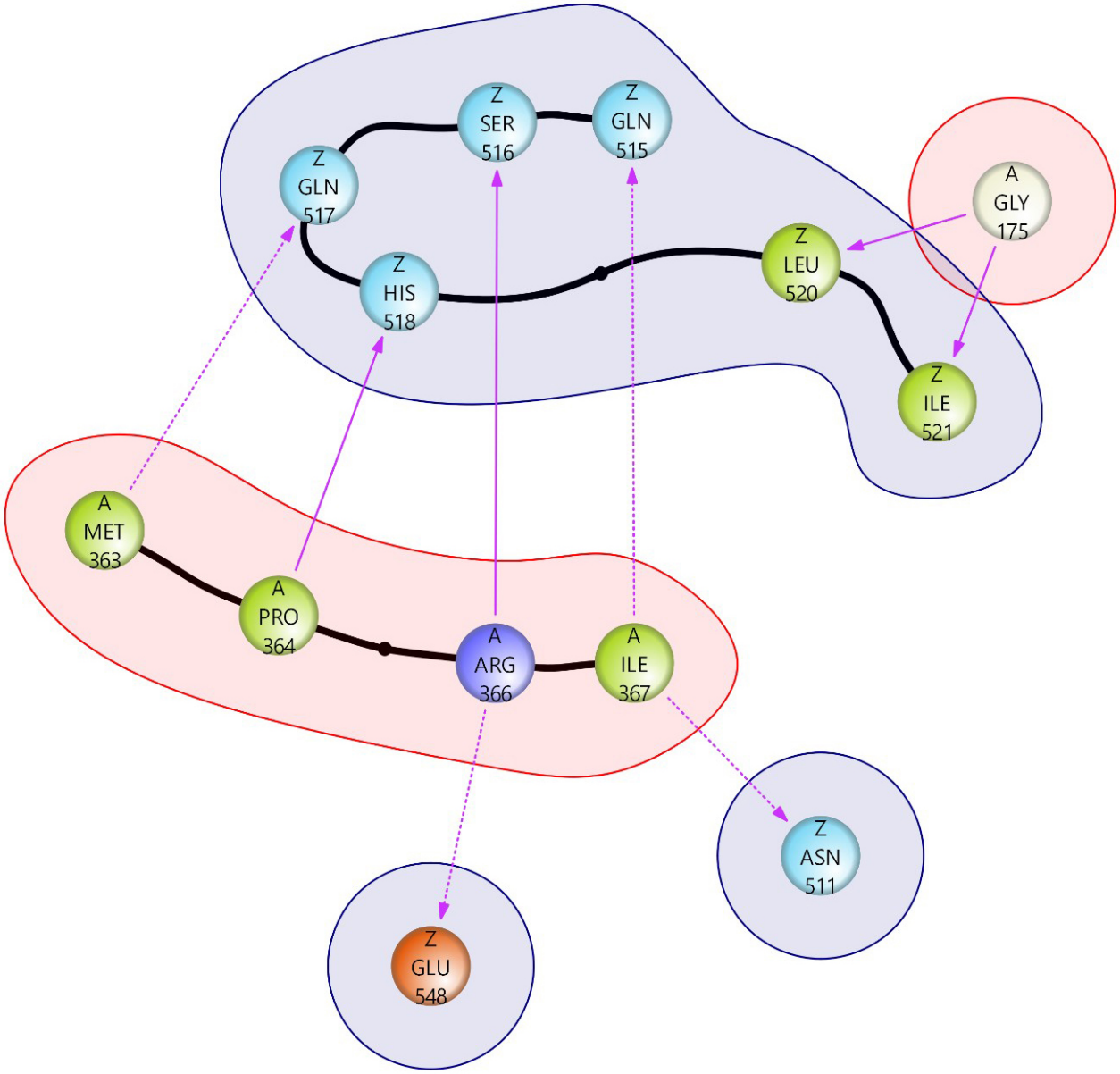

Fig. 10. 2D interaction maps of the CTD-ngMutL:ngβ interface illustrating the structural consequences of cysteine substitutions. The interaction network of the cysteine-free variant after MD simulation. Chain A (β-clamp monomer 1) is shown in red, chain Z (CTD monomer 1, non-catalytic) in purple. Magenta solid and dotted arrows indicate hydrogen bonds involving backbone and side-chain atoms, respectively, pointing from the hydrogen bond donor to the acceptor.

cessing. This separation of binding and catalytic functions is difficult to achieve with wild-type protein and makes ngMutL^{cf} a promising tool for mechanistic dissection of the alternative DNA-binding properties of ngMutL, including its interactions with the *pilE* G4 and their potential role in gonococcal pathogenesis.

5. Limitations

Several limitations of the present study should be acknowledged. First, regarding the molecular dynamics simulations: the MD trajectories were initiated from a single starting conformation (PDB: 8XLA) and the simulation time (1.2 ns) was limited, which restricts conformational sampling. While the observed displacement of the catalytic residues and loss of interface contacts in the Cys-free variant are internally consistent and supported by experimental data, longer simulations and ensemble averaging would be required to obtain quantitative thermodynamic parameters such as binding free energies. The MD simulations were performed on the protein complex alone, without explicit metal cofactors (Mn^{2+}/Mg^{2+}) or a DNA substrate. Both are known to influence protein conformation

and interfacial dynamics: divalent cations stabilize the active site geometry, while the presence of DNA threading through the β-clamp channel would impose additional geometric constraints on the MutL-CTD: β-clamp complex and could alter the relative positioning of the two CTD monomers. Inclusion of these components in future simulations would provide a more complete picture of the productive and non-productive binding modes. Second, the endonuclease assays on linear substrates were performed under supraphysiological Mn^{2+} concentrations (5 mM), which were necessary to observe robust activity *in vitro*. While this does not affect the comparative conclusions both variants were assayed under identical conditions — extrapolation to physiological metal concentrations should be made with caution. Finally, all biochemical experiments were performed *in vitro* with purified components. The behavior of $ngMutL^{cf}$ in the cellular context, where additional protein partners, DNA topology, and post-translational modifications may influence activity, remains to be investigated.

6. Conclusions

In this study, we performed a comprehensive biochemical, biophysical, and computational characterization of wild-type ngMutL and a Cys-free variant from the *Neisseria gonorrhoeae* mismatch repair system. We demonstrate that the replacement of all five Cys residues does not affect the global secondary structure of the protein, its ATPase activity, DNA-binding capacity, or endonuclease activity on supercoiled plasmid substrates. However, cysteine substitutions lead to a near-complete loss of sliding clamp-dependent endonuclease activity on linear DNA duplexes.

Molecular dynamics simulations initiated from the crystal structure of the complex C-terminal domain MutL with β-clamp (PDB: 8XLA) reveal that this functional deficiency has a precise structural basis. In the wild-type complex, the catalytically active CTD monomer engages the β-clamp through multiple stabilizing contacts, including a specific hydrogen bond. In the Cys-free variant, the catalytically active monomer is involved in the formation of weaker van der Waals contacts with the clamp interface, and the catalytic residues D491, H493, and E497 are displaced by 14–17 Å relative to their position in the wild-type complex—a shift sufficient to prevent productive orientation of the daughter strand towards the active site. These results demonstrate that Cys residues of ngMutL are not directly involved in catalysis but are essential for maintaining the conformational rigidity of the C-terminal domain required for productive engagement with the sliding clamp and correct geometric positioning of the catalytic monomer—the key determinant of strand discrimination in methylation-independent MMR.

Beyond this, the Cys-free variant characterized here represents a valuable biochemical tool. Since $ngMutL^{cf}$ retains DNA-binding capacity and ATPase activity while being specifically deficient in sliding clamp-dependent endonuclease activity on linear substrates, it enables the study of any DNA recognition or protein interaction event mediated by ngMutL in the absence of productive strand cleavage. This functional uncoupling is difficult to achieve with the wild-type protein and opens the way for mechanistic investigation of the full spectrum of non-canonical activities of ngMutL—including its interactions with G-quadruplex structures, its potential role in the regulation of pilin antigenic variation, and other functions that may yet be discovered.

Availability of Data and Materials

All data reported in this paper will also be shared by the corresponding author upon request.

Author Contributions

EAK and VYS designed the research study. VYS, VGS, MVM, DRB and AVL performed the research. EAK and TSO provided help and advice on planning and performance of experiments. VYS, MVM and VGS analyzed the data. VYS, VGS and TSO wrote the manuscript. VYS, VGS and TSO prepared figures and tables and conducted references collection. All authors contributed to editorial changes in the manuscript. All authors read and approved the final manuscript. All authors have participated sufficiently in the work and agreed to be accountable for all aspects of the work.

Ethics Approval and Consent to Participate

Not applicable.

Acknowledgment

The authors thank professor D.N. Rao (Department of Biochemistry, Indian Institute of Science) for kindly providing the plasmid constructs encoding the recombinant wild-type and cysteine-free MutL proteins.

Funding

This work was carried out and supported as part of the scientific project of the state assignment of Lomonosov Moscow State University.

Conflicts of Interest

The authors declare no conflicts of interest.

Declaration of AI and AI-Assisted Technologies in the Writing Process

During the preparation of this work, the authors used Claude in order to check spelling and grammar. After using this tool, the authors reviewed and edited the content as needed and take full responsibility for the content of the publication.

Supplementary Material

Supplementary material associated with this article can be found, in the online version, at https://doi.org/10.31083/FBL55117.

References

[1] Nirwal S, Jha R, Narayanan N, Sharma M, Kulkarni DS, Sharma D, et al. The structure of the MutL-CTD:processivity-clamp complex provides insight regarding strand discrimination in non-methyl-directed DNA mismatch repair. Nucleic Acids Research. 2025; 53: gkaf094. https://doi.org/10.1093/nar/gkaf094

[2] Hill SA, Masters TL, Wachter J. Gonorrhea - an evolving disease of the new millennium. Microbial Cell (Graz, Austria). 2016; 3: 371–389. https://doi.org/10.15698/mic2016.09.524

[3] Cahoon LA, Seifert HS. Focusing homologous recombination: pilin antigenic variation in the pathogenic Neisseria. Molecular Microbiology. 2011; 81: 1136–1143. https://doi.org/10.1111/j.1365-2958.2011.07773.x

[4] Criss AK, Bonney KM, Chang RA, Duffin PM, LeCuyer BE, Seifert HS. Mismatch correction modulates mutation frequency and pilus phase and antigenic variation in Neisseria gonorrhoeae. Journal of Bacteriology. 2010; 192: 316–325. https://doi.org/10.1128/JB.01228-09

[5] Rotman E, Seifert HS. Neisseria gonorrhoeae MutS affects pilin antigenic variation through mismatch correction and not by pilE guanine quartet binding. Journal of Bacteriology. 2015; 197: 1828–1838. https://doi.org/10.1128/JB.02594-14

[6] Cahoon LA, Seifert HS. An alternative DNA structure is necessary for pilin antigenic variation in Neisseria gonorrhoeae. Science (New York, N.Y.). 2009; 325: 764–767. https://doi.org/10.1126/science.1175653

[7] Savitskaya VY, Strekalovskikh VV, Snyga VG, Monakhova MV, Arutyunyan AM, Dolinnaya NG, et al. *pilE* G-Quadruplex Is Recognized and Preferentially Bound but Not Processed by the MutL Endonuclease from *Neisseria gonorrhoeae* Mismatch Repair Pathway. International Journal of Molecular Sciences. 2023; 24: 6167. https://doi.org/10.3390/ijms24076167

[8] Duppatla V, Bodda C, Urbanke C, Friedhoff P, Rao DN. The C-terminal domain is sufficient for endonuclease activity of Neisseria gonorrhoeae MutL. The Biochemical Journal. 2009; 423: 265–277. https://doi.org/10.1042/BJ20090626

[9] Namadurai S, Jain D, Kulkarni DS, Tabib CR, Friedhoff P, Rao DN, et al. The C-terminal domain of the MutL homolog from Neisseria gonorrhoeae forms an inverted homodimer. PloS One. 2010; 5: e13726. https://doi.org/10.1371/journal.pone.0013726

[10] Guarné A, Charbonnier JB. Insights from a decade of biophysical studies on MutL: Roles in strand discrimination and mismatch removal. Progress in Biophysics and Molecular Biology. 2015; 117: 149–156. https://doi.org/10.1016/j.pbiomolbio.2015.02.002

[11] Correa EME, Martina MA, De Tullio L, Argaraña CE, Barra JL. Some amino acids of the Pseudomonas aeruginosa MutL D(Q/M)HA(X)(2)E(X)(4)E conserved motif are essential for the in vivo function of the protein but not for the in vitro endonuclease activity. DNA Repair. 2011; 10: 1106–1113. https://doi.org/10.1016/j.dnarep.2011.08.007

[12] Monakhova MV, Milakina MA, Savitskaia VY, Romanova EA, Rao DN, Kubareva EA. MutL Protein from the Neisseria gonorrhoeae Mismatch Repair System: Interaction with ATP and DNA. Molekuliarnaia Biologiia. 2021; 55: 289–304. https://doi.org/10.31857/S0026898421020117

[13] Pavlova AV, Savitskaya VY, Dolinnaya NG, Monakhova MV, Litvinova AV, Kubareva EA, et al. G-Quadruplex Formed by the Promoter Region of the *hTERT* Gene: Structure-Driven Effects on DNA Mismatch Repair Functions. Biomedicines. 2022; 10: 1871. https://doi.org/10.3390/biomedicines10081871

[14] Fukui K, Nishida M, Nakagawa N, Masui R, Kuramitsu S. Bound nucleotide controls the endonuclease activity of mismatch repair enzyme MutL. The Journal of Biological Chemistry. 2008; 283: 12136–12145. https://doi.org/10.1074/jbc.M800110200

[15] Kosinski J, Plotz G, Guarné A, Bujnicki JM, Friedhoff P. The PMS2 subunit of human MutLalpha contains a metal ion binding domain of the iron-dependent repressor protein family. Journal of Molecular Biology. 2008; 382: 610–627. https://doi.org/10.1016/j.jmb.2008.06.056

[16] Laitaoja M, Valjakka J, Jänis J. Zinc coordination spheres in protein structures. Inorganic Chemistry. 2013; 52: 10983–10991. https://doi.org/10.1021/ic401072d

[17] Dalton K, Lopez T, Pande V, Frydman J. REP-X: An Evolution-guided Strategy for the Rational Design of Cysteine-less Protein Variants. Scientific Reports. 2020; 10: 2193. https://doi.org/10.1038/s41598-020-58794-x

[18] Kipper K, Eremina N, Marklund E, Tubasum S, Mao G, Lehmann LC, et al. Structure-guided approach to site-specific fluorophore labeling of the lac repressor LacI. PloS One. 2018; 13: e0198416. https://doi.org/10.1371/journal.pone.0198416

[19] Giron-Monzon L, Manelyte L, Ahrends R, Kirsch D, Spengler B, Friedhoff P. Mapping protein-protein interactions between MutL and MutH by cross-linking. The Journal of Biological Chemistry. 2004; 279: 49338–49345. https://doi.org/10.1074/jbc.M409307200

[20] Monakhova MV, Penkina AI, Pavlova AV, Lyaschuk AM, Kucherenko VV, Alexeevski AV, et al. Endonuclease Activity of MutL Protein of the Rhodobacter sphaeroides Mismatch Repair System. Biochemistry. Biokhimiia. 2018; 83: 281–293. https://doi.org/10.1134/S0006297918030082

[21] Ban C, Yang W. Crystal structure and ATPase activity of MutL: implications for DNA repair and mutagenesis. Cell. 1998; 95: 541–552. https://doi.org/10.1016/s0092-8674(00)81621-9

[22] Pillon MC, Miller JH, Guarné A. The endonuclease domain of MutL interacts with the β sliding clamp. DNA Repair. 2011; 10: 87–93. https://doi.org/10.1016/j.dnarep.2010.10.003

[23] Pillon MC, Babu VMP, Randall JR, Cai J, Simmons LA, Sutton MD, et al. The sliding clamp tethers the endonuclease domain of MutL to DNA. Nucleic Acids Research. 2015; 43: 10746–10759. https://doi.org/10.1093/nar/gkv918

[24] Han XP, Yang XW, Liu J. MutS and MutL sliding clamps in DNA mismatch repair. Genome Instability & Disease. 2023; 4: 1–11. https://doi.org/10.1007/s42764-022-00094-x